Astron. Astrophys. 338, 556–562 (1998)

ASTRONOMY AND ASTROPHYSICS

# Progressive covering in dipping and Comptonization in the spectrum of XB 1916-053 from the BeppoSAX observation

**M.J. Church[1], A.N. Parmar[2], M. Bałucińska-Church[1], T. Oosterbroek[2], D. Dal Fiume[3], and M. Orlandini[3]**

[1] School of Physics and Astronomy, University of Birmingham, Birmingham, B15 2TT, UK
(mjc@star.sr.bham.ac.uk; mbc@star.sr.bham.ac.uk)
[2] Astrophysics Division, Space Science Department of ESA, ESTEC, Postbus 299, 2200 AG Noordwijk, The Netherlands
(aparmar@astro.estec.esa.nl; toosterb@astro.estec.esa.nl)
[3] Istituto TESRE, CNR, via Gobetti 101, I-40129 Bologna, Italy
(daniele@tesre.bo.cnr.it; orlandini@tesre.bo.cnr.it)

Received 27 February 1998 / Accepted 26 May 1998

**Abstract.** We report results of a BeppoSAX observation of the low-mass X-ray binary (LMXB) dipping source XB 1916−053. The source joins the small group of LMXB detected at energies $\gtrsim$100 keV. The non-dip spectrum is well fitted by an absorbed blackbody with a temperature of $1.62\pm0.05$ keV and an absorbed cut-off power law with a photon index of $1.61\pm0.01$ and a cut-off energy of $80\pm10$ keV. Below 10 keV, where photoelectric absorption is dominant, the dramatic spectral changes observed during dips can be simply modelled by progressive covering of the blackbody and cut-off power law components. The blackbody component is very rapidly absorbed during dips, consistent with it being point-like, while the cutoff power law is more gradually absorbed, consistent with it being extended. The most likely locations for the blackbody component are the surface of the neutron star or the boundary layer between the neutron star and the accretion disk. The extended emission most probably originates in an accretion disk corona. Above 10 keV, dipping is detected up to $\sim$40 keV, and there is some evidence for an energy-independent reduction in intensity of up to 15%. This reduction could be caused by electron scattering or obscuration. In the first case, the change is consistent with an electron column density of $\sim 2.9 \times 10^{23}$ cm$^{-2}$, several times smaller than the average hydrogen column measured simultaneously.

**Key words:** X-rays: stars – stars: individual: XB 1916-053 – stars: neutron – binaries: close – accretion: accretion discs

## 1. Introduction

XB 1916−053 is a member of the class of Low Mass X-ray Binaries that exhibit irregular reductions, or dips, in X-ray intensity which repeat at the orbital period. It is generally accepted that these dips are due to obscuration in the thickened outer regions of a disk where the accretion flow from the companion star impacts. XB 1916−053 has the shortest period of all dipping sources of 50 min (Walter et al. 1982), and is also notable because of the difference of $\sim$1% between the X-ray and optical periods (Grindlay et al. 1988). The source is a member of the sub-group of dipping sources in which the spectral evolution has been fitted by an "absorbed plus unabsorbed" approach, also used for XBT 0748−676 and XB 1254−690 (Parmar et al. 1986; Courvoisier et al. 1986). In this approach, the non-dip spectrum in the band 1–10 keV is fitted by a simple absorbed power-law or absorbed cut-off power law model. However during dipping intervals, two spectral components are evident; one absorbed and the other not. It has been customary to fit these spectra by dividing the non-dip model into two parts, each having the power law index of the non-dip spectrum, one of which is absorbed, and the other having the non-dip column density. However, the normalization of the unabsorbed component decreases markedly (e.g., Smale et al. 1988), and the explanation of this is not obvious. It has been suggested that the unabsorbed part of the spectrum is due to electron scattering in the absorber.

The dipping LMXB sources do not, in general, show the spectral evolution expected for absorption by cold material, ie a hardening of the spectrum as lower energies are preferentially removed. Some sources show energy independence, eg, X 1755−338 (White et al. 1984; Church & Bałucińska-Church 1993). X 1624−490 shows a strong softening in deep dipping (Church & Bałucińska-Church 1995). The absorbed plus unabsorbed sources have strong unabsorbed components. This complexity is not predicted by the models where the dips are due to simple absorption of a point source by neutral material. However it has been possible to explain the spectral evolution in all of these sources using the model proposed by Church & Bałucińska-Church (1995), in which the emission consists of point-like blackbody emission from the surface of the neutron star, plus an extended Comptonized component from an accretion disk corona. In the ASCA observation of XB 1916−053 dipping was $\sim$100% deep in the 1–10 keV band, showing that all emission components were removed, and good fits to dip data were obtained using the two-component model including *progressive* covering of the extended emission region (Church et al. 1997). This suggests a new explanation for the absorbed and un-

*Send offprint requests to*: M.J. Church

absorbed sources in which a large, dense absorber moves across the source, so that the covering fraction increases smoothly from zero to unity. The unabsorbed peak is simply the uncovered part of the extended emission at any stage of dipping, and with this modelling good fits can be obtained below 10 keV, without the need for substantial electron scattering or unusual abundances of the absorbing material. Furthermore, calculations of the relative losses of X-ray intensity in the absorber due to photoelectric absorption and electron scattering showed that, below 10 keV, little scattering is expected for cosmic abundances (Church et al. 1997). This is not the case above 10 keV where the Thomson cross section becomes larger than that of photoelectric absorption.

XB 1916−053 has been observed with OSO-8 and *Ginga* above 10 keV. From the OSO-8 results of White & Swank (1982) it is clear that dipping persisted up to ∼20 keV. In the case of the *Ginga* data (Smale et al. 1992), it is unclear from the published results up to what energy dipping continued. XB 1916−053 was not detected by OSSE (Barret et al. 1996). Until recently, there has been little investigation of LMXB above 10 keV, although there is evidence from *Sigma* results that the spectra of several low luminosity burst sources extend to high energies (Barret & Vedrenne 1994). It is clearly important to investigate the spectra of LMXB at high energies. In the case of XB 1916−053 we show for the first time that the spectrum extends to above 100 keV, that a Comptonization break has been seen for the first time in a dipping source, and that dipping persists to high energies.

## 2. Observations

Results from the Low-Energy Concentrator Spectrometer (LECS; 0.1–10 keV; Parmar et al. 1997), Medium-Energy Concentrator Spectrometer (MECS; 1.3–10 keV; Boella et al. 1997) and the Phoswich Detection System (PDS; 15–300 keV; Frontera et al. 1997) on-board BeppoSAX are presented. The MECS consists of three identical grazing incidence telescopes with imaging gas scintillation proportional counters in their focal planes. The LECS uses an identical concentrator system as the MECS, but utilizes an ultra-thin (1.25 $\mu$m) entrance window and a driftless configuration to extend the low-energy response to 0.1 keV. The fields of view of the LECS and MECS are circular with diameters of 37′and 56′, respectively. The non-imaging PDS consists of four independent units arranged in pairs each having a separate collimator. Each collimator can be alternatively rocked on- and off-source to monitor the background counting rate. The hexagonal PDS field of view is 78′ full-width at half maximum.

The region of sky containing XB 1916−053 was observed by BeppoSAX between 1997 April 27 21:00 and April 28 19:51 UTC in an observation lasting 80 ks and spanning 27 orbital cycles. Good data were selected from intervals when the elevation angle above the Earth's limb was $>4^\circ$ and when the instrument configurations were nominal, using the SAXDAS 1.3.0 data analysis package. The standard PDS collimator rocking angle of 210′, and standard dwell time of 96 s for each on- and off-source position were used. LECS is operated only during satellite night-time resulting in decreased exposure. LECS and MECS data were extracted centered on the position of XB 1916−053 using radii of 8′ and 4′, respectively. Background subtraction in the imaging instruments was performed using standard files, but is not critical for this source. Background subtraction in the PDS was carried out using data from the offset detectors.

## 3. Results

### *3.1. Light curves and hardness ratio*

The light curves of all 3 instruments reveal dipping; in the LECS and MECS dipping is very strong, however dipping was also apparent in the PDS. Fig. 1 shows the MECS 1.65–10 keV light curve after background subtraction. Coverage of dipping is very good, with complete coverage of 11 dips with associated non-dip data. However in the central part of the observation several dips were only partially observed. Dipping is very deep, reaching close to 100% in all of the dips observed. This shows that the absorber is both dense and extended in relation to all source regions. The reduced exposure of the source in the LECS resulted in coverage of non-dip data, dip ingress and deep dipping, but with little egress data.

The best-fit orbital period was obtained using MECS data in which dip coverage was better. The data were folded on test periods in the range 2940–3060 s, and a best value of 3002±6 s obtained. The errors are based on the uncertainty in the location of the peak of the $\chi^2$ *versus* period plot produced by the period searching program. Because of the variable nature of the dipping in shape, depth and width, it is possible that the errors may be underestimated. The value of 3002±6 s is consistent with previous determinations of 3015±17 s (*Exosat*, Smale et al. 1989), 3005±6.6 s (*Ginga*, Smale et al. 1992) and 3005±20 s (ASCA, Church et al. 1997).

Fig. 2 shows folded background subtracted light-curves in the energy ranges 1.0–2.0 keV and 4.0–10.0 keV, together with the hardness ratio derived from these. Dipping is 98% deep in the band 1.0–2.0 keV, but becoming 100% at times, and 89% deep in the 4.0–10.0 keV energy range. Thus, there is a clear energy dependence of the dipping, also shown by the width of dipping in the two bands. In the lower energy range, dipping is very broad and flat-bottomed showing that the increase in column density is sufficient to reduce the count rate rapidly to close to zero, which then persists for an interval of 0.2 in phase. In the higher energy band, the count rate continues to fall to a minimum value at the center of dipping. In both bands, the width of dipping is 0.39 in phase, equivalent to the absorber subtending a large angle of 140° at the neutron star. Interdipping, at phases between the main dips, can be seen in the lower band, and in the raw light curve can be as deep as 60%; however it appears to be variable in depth and in phase and so is smeared out in the folding. The increase in hardness ratio in dip ingress and egress show that part of the spectrum is being removed at low energies, although the spectrum is complicated by the presence of an unabsorbed peak as discussed below.

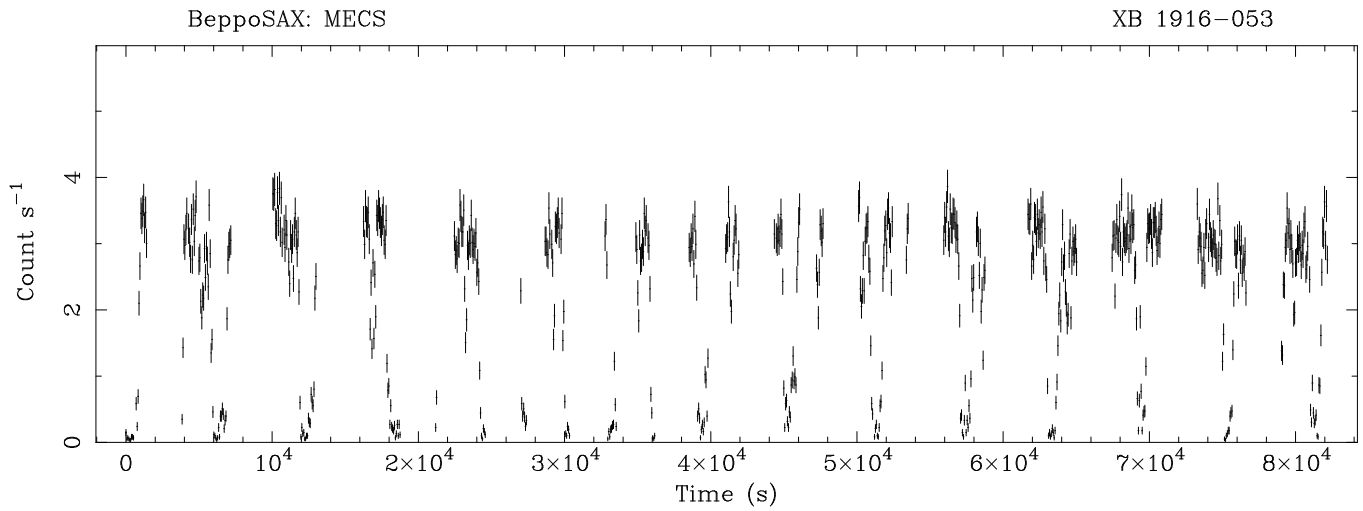


**Fig. 1.** Light curve of the complete BeppoSAX observation of XB 1916−053 in 64 s bins from merged MECS data in the energy band 1.65–10.0 keV

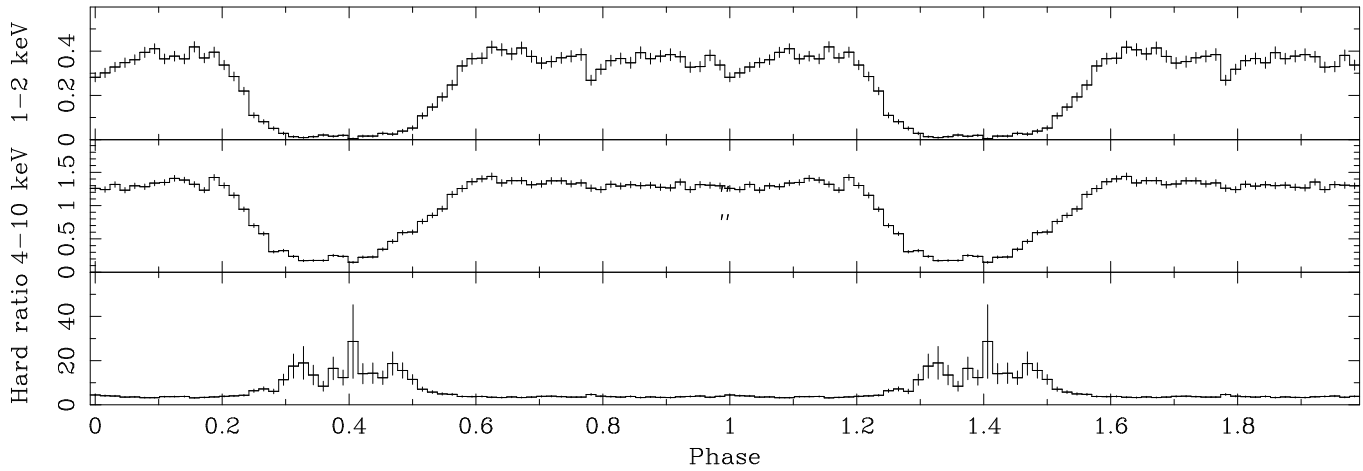


**Fig. 2.** Folded MECS light curves: counts s$^{-1}$ in the bands 1–2 keV and 4–10 keV and the hardness ratio

### *3.2. The broad-band spectrum*

The spectrum of non-dip emission was investigated by simultaneously fitting LECS, MECS and PDS data. LECS data were selected with count rate greater than 1.2 s$^{-1}$, MECS data were selected between 3.1 and 4.0 counts s$^{-1}$, and PDS data were selected using the time filters derived from the MECS selection.

LECS and MECS data were rebinned to a minimum of 20 counts per channel giving 392 and 217 channels, respectively. PDS data were rebinned to 15 channels spanning the range 13–200 keV. Response functions appropriate to the extraction radii in LECS and MECS, and to the rebinning in the PDS were used. Responses from Sept. 1997 were used for the MECS and PDS, and the improved response of Feb. 1998 used for LECS. Factors were applied in the fitting to allow for known normalization differences between the instruments, the LECS and PDS requiring values of ∼0.95 and ∼0.90 relative to the MECS, respectively. LECS data were used in the band 0.1–10.0 keV, and MECS data between 1.65–10.0 keV, where the calibration is well established. The photoelectric absorption coefficients of Morrison & McCammon (1983) together with the solar abundances of Anders & Grevesse (1989) were used throughout.

Initially, simple models were tested, including an absorbed power law. There were clear signs of downcurving in the spectrum above ∼35 keV and so channels above this energy were ignored. The fit was still unacceptable with a $\chi^2$ of 789 for 512 degrees of freedom (dof). An absorbed cut-off power law also gave an unacceptable fit, with a lower $\chi^2$ of 609 for 522 dof. The spectrum was fitted acceptably below 10 keV, but with large systematic deviations of the model below the data above 30 keV. This was due to the curvature in the spectrum between 1 and 10 keV being modelled by Comptonization down-curving (via a low cut-off energy $E_{CO}$ ∼20 keV), clearly incorrect. A two-component model consisting of a blackbody as well as non-thermal emission was tried, since this has been previously applied to several dipping sources. In this previous work, data was not available above 10 keV, and a power law was used to represent Comptonization at energies $\ll E_{CO}$, the cut-off energy. With BeppoSAX, this approximation cannot be used, and

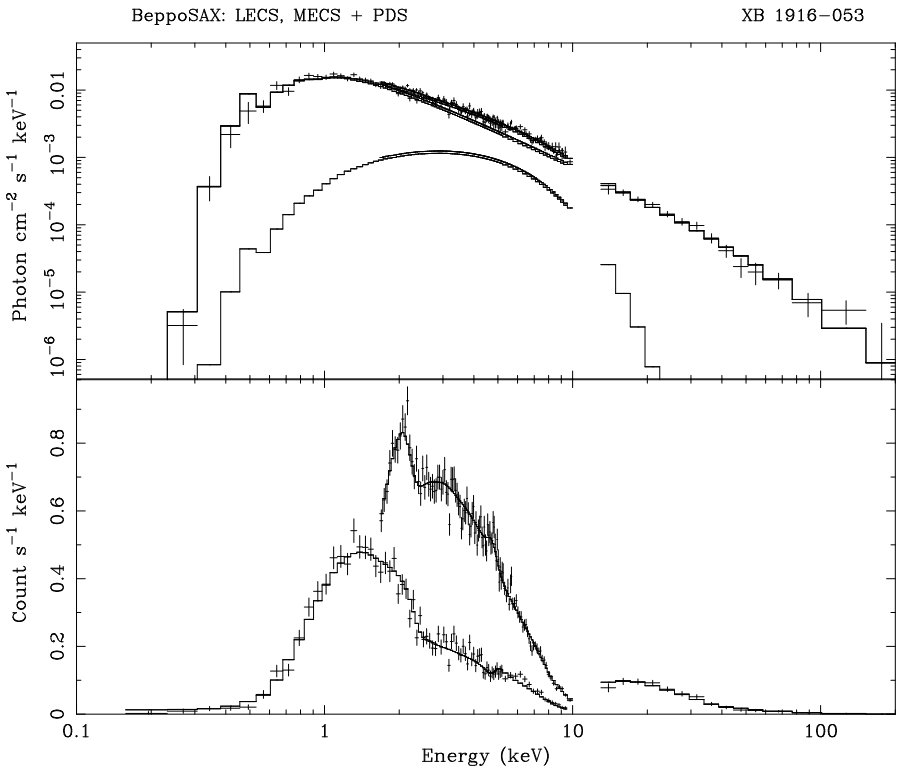


**Fig. 3.** The broad-band non-dip spectrum from the LECS, MECS and PDS. The unfolded spectrum (top) shows the individual blackbody, cut-off power law and total spectral components, but in the folded spectrum only the total model is shown

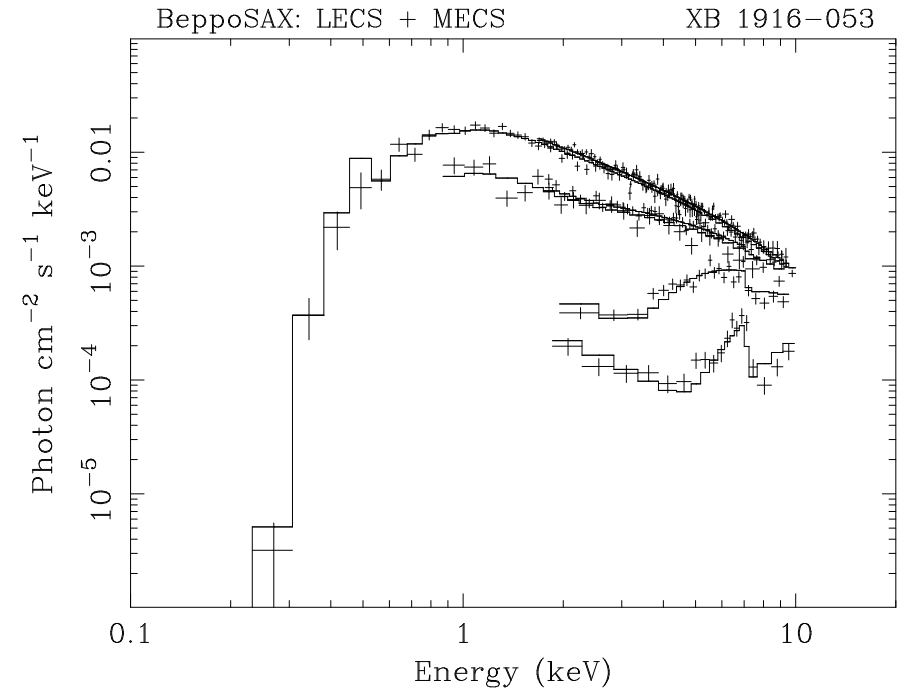


**Fig. 4.** Non-dip, intermediate dip and deep dip spectra fitted by the best-fit models discussed in the text

**Table 1.** (a) Parameters of the broadband non-dip spectrum: $N_H$ is in units of $10^{22}$ H atom $cm^{-2}$, $E_{CO}$ is the cut-off energy; 90% confidence uncertainties are given. (b) The quality of the fit with the blackbody component removed

| | $N_H$ | kT (keV) | $\Gamma$ | $E_{CO}$ (keV) | $\chi^2$/dof |
|---|---|---|---|---|---|
| a | $0.32 \pm 0.02$ | $1.62 \pm 0.05$ | $1.61 \pm 0.01$ | 80.4±10.0 | 537/520 |
| b | $0.32 \pm 0.02$ | ... | 1.61 | 80.4 | 2270/525 |

a model of the form: AB*(BB + CPL) was tried, where AB is an absorption term, and BB and CPL are the blackbody and cut-off power law components. This gave a good fit to the non-dip spectrum, with a $\chi^2$ of 537 for 520 dof, and results are shown in Table 1(a) and Fig. 3. The blackbody component has an unabsorbed 1–10 keV flux of $4.8 \times 10^{-11}$ erg cm$^{-2}$ s$^{-1}$, 19.5% of the total flux in this band. Compared with the absorbed cut-off power law model, an F-test indicates that the inclusion of the blackbody is significant at $\gg$99.9% confidence. A better test of the significance was made by re-fitting the absorbed cut-off power law, forcing a good fit above 10 keV by fixing $\Gamma$ and $E_{CO}$ to the two-component model values. The curvature in the spectrum between 1 and 10 keV was badly fitted by the cut-off power law without a blackbody, giving a $\chi^2$/dof of 2270/525 as shown in Table 1(b).

We also fitted the LECS and MECS data without the PDS, to investigate whether using the standard, but relatively narrow band, stopping at 10 keV affects the spectral fitting results. Using a cut-off power law model, the value of $\Gamma$ was found to be $\sim$1.75, with $kT_{bb}$ = 1.75 keV and $\chi^2$ = 525 for 505 dof. Fitting a simple power law model, on the basis that Comptonization down-curving is small $\ll$ the cut-off energy, gives similar values of $\Gamma$, ie there is little additional error in using the simple power law. It is thus clear that in a restricted energy band, there is a tendency to overestimate the power law index, which is about 10% in the case of XB 1916−053 . The reason for the effect is probably that there are two sources of curvature in the spectrum: the blackbody and Comptonization. Without high energy data, the blackbody contribution may be overestimated, steepening the measured power law index.

### *3.3. Spectral Evolution during dipping*

Dip intervals were selected based on intensity selection of the MECS data, and time filters corresponding to these selections used to make LECS spectra. Various intensity bands were tried using up to 7 contiguous bands, and spectral fitting performed. The final results are shown in Fig. 4 with 4 non-contiguous bands only, for clarity. A model of the form: AB*BB + AG*PCF*CPL was used, where AG is the non-dip absorption term and PCF is partial covering, ie the two-component model which gave good fits to the non-dip broad-band spectrum, but allowing progressive covering of the extended emission (see Sect. 1). It is possible to fit LECS and MECS data simultaneously only for non-dip and the 1st dip spectrum shown in Fig. 4, since in deeper dipping insufficient LECS counts are available and only MECS data were fitted. PDS data would not help clarify the complex changes occurring in the 1–10 keV energy range. The best-fit parameters of the non-dip spectrum: $kT_{bb}$, $\Gamma$, $E_{CO}$ and the normalizations were fixed in fitting the dip spectra, and good fits were obtained. Fig. 4 shows that the dip spectra clearly display the presence of a strong unabsorbed peak which is well-modelled as the uncovered part of the extended Comptonized emission at all levels of dipping.

Difficulty was initially found in fitting the deepest dip spectrum in the merged MECS data which had been selected in the intensity band 0.0–0.45 counts s$^{-1}$. Poor fits were obtained with values of reduced $\chi^2$ of $\sim$3. When the intensity band was divided into two, strong spectral changes were found between these bands, and the lower band between 0.0–0.3 counts s$^{-1}$ could be fitted acceptably. Fig. 4 shows the fit to 4 intensity levels selected in the bands: 0.0–0.3, 0.4–0.8, 1.6–2.2, and 3.1–4.0 counts s$^{-1}$, and the corresponding fit parameters are given in Table 2. Fig. 5 shows plots against intensity of the covering fraction, and the blackbody and cut-off power law column densities for all 7 intensity bands.

It can be seen that the blackbody column densities increase rapidly, and have larger values than the Comptonized emission at every level, consistent with the point source blackbody measuring $N_H$ along a localized track, whereas the $N_H$ of the Comptonized emission is an average appropriate to an extended emission region covered by extended absorber with a density gradient. Fig. 5 shows that the partial covering fraction *f* increases smoothly from zero to close to unity demonstrating that the source regions are progressively covered by dense absorber, and showing that the model provides a simple explanation of the complex spectral changes observed during dipping.

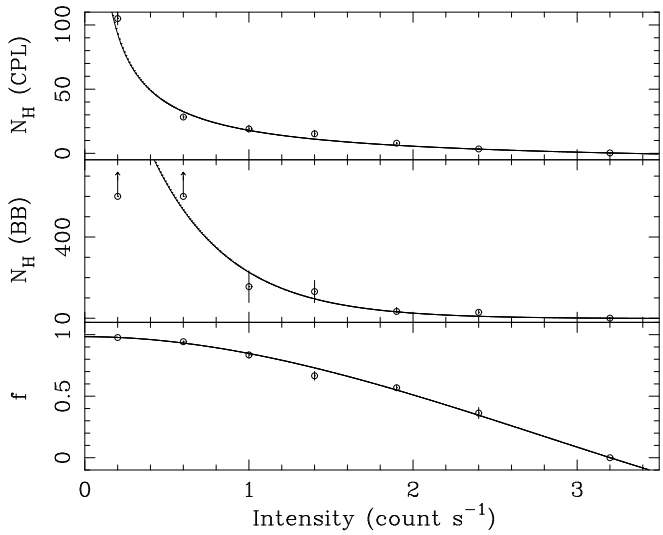


**Fig. 5.** The covering fraction *f* of the extended non-thermal spectral component as a function of source intensity, together with the column densities of the backbody and cut-off power law in units of $10^{22}$ H atom cm$^{-2}$. At the lowest two dip intensities, the blackbody column densities are lower limits

**Table 2.** Best fits to the dip spectra shown in Fig. 4: $N_H$ is in units of $10^{22}$ H atom cm$^{-2}$ for the blackbody and cut-off power-law components; *f* is the covering fraction, and 90% confidence limits are given

| intensity (count s$^{-1}$) | $N_H^{BB}$ | $N_H^{CPL}$ | f |
|---|---|---|---|
| non-dip | 0.32 | 0.32 | 0. |
| 1.6–2.2 | 33±20 | 7.9±0.8 | 0.569±0.020 |
| 0.4–0.8 | >600 | 28.4±1.5 | 0.943±0.007 |
| 0.0–0.3 | >600 | 105±5 | 0.977±0.003 |

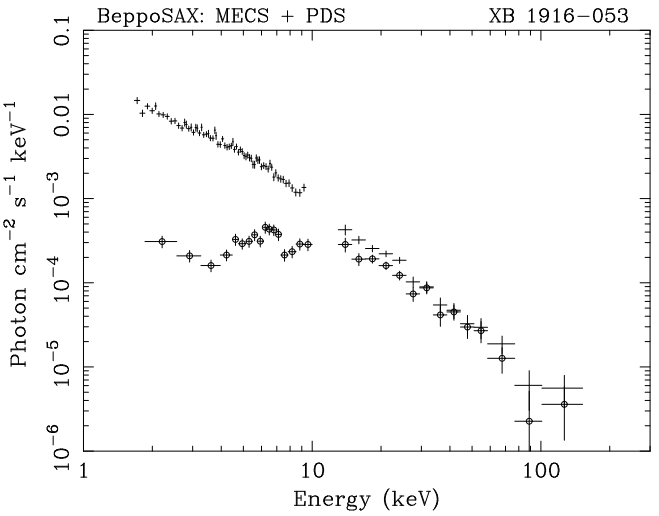


**Fig. 6.** Non-dip and deep dip spectra from the MECS1 and PDS instruments showing dipping persisting to high energies

Next, we compared the non dip and deep dip spectrum using MECS and PDS data, ie concentrating on the spectrum above 1 keV. PDS deep dip data were selected using time filters derived from the MECS, since the dips are not clearly visible in the PDS. The main result (Fig. 6) is a systematic reduction in flux in the deep dip PDS spectrum compared with the non-dip interval. The cut-off power law model was fitted to the non-dip PDS data with the best-fit non-dip parameters. The same model was applied to the deep dip PDS spectrum, but with the appropriate partial covering fraction and column density derived from the low-energy fits. These parameters do not influence the spectrum above ∼20 keV. Consequently, an additional scaling factor was allowed between the deep dip and non-dip spectra. Without this factor the $\chi^2$ was 27.2 for 13 dof. The best fit value of the scaling factor was 0.84 giving a $\chi^2$ of 11.3 for 13 dof. Photoelectric absorption will have effects above 10 keV however, and Fig. 6 does not represent an unambiguous detection of electron scattering.

## 4. Discussion

We have observed the LMXB dipping source XB 1916−053 in the very broad energy range of 0.1–200 keV, using the LECS, MECS and PDS instruments on BeppoSAX. We find that the spectrum extends to the highest energies of the PDS, and is a striking example of a LMXB with a strong high energy component. Moreover, comparison of the non-dip and deep dip spectra reveals that dipping is most marked in the 0.1–10 keV range, but also that there are significant reductions of flux up to ∼40 keV, and some evidence, although not conclusive, for an energy-independent reduction in PDS flux. Dipping at high energies must be due either to electron scattering or to obscuration of the source by a very dense absorber. If the dipping is due to electron scattering, then the reduction factor is $\exp\ -(\mathrm{N_e}\sigma_\mathrm{T})$ where $\sigma_T$ is the Thomson scattering cross section, = $6.7 \times 10^{-25}$ cm$^2$. Thus, the average electron column density $\mathrm{N_e}$ has the value $2.6 \times 10^{23}$ cm$^{-2}$ for a reduction factor of 0.84, several times smaller than the largest average value of $\mathrm{N_H}$. We can estimate the value of the ionization parameter $\xi$ in the absorbing bulge using the luminosity of the source. During this observation, the source was relatively faint with L$\sim 6 \times 10^{36}$ erg s$^{-1}$ in the energy range 0.5–200 keV for a distance ∼9 kpc. Using column densities derived at various levels of dipping, $\xi$ varies from a maximum of ∼50 at the outer edges to <1 in the center of the absorber, implying a low ionization state throughout the absorber. The difference between $\mathrm{N_e}$ and $\mathrm{N_H}$ also indicates that part of the absorber may be not significantly ionized.

Next, we find that the non-dip spectrum can be well described by the model in which the emission consists of point-source blackbody emission from the neutron star plus extended Comptonized emission from the accretion disk corona as proposed by Church & Bałucińska-Church (1995). This is the first time for this source, and the first time for dipping source in general, that the energy band of the instruments includes $\mathrm{E_{CO}}$. Values of $\mathrm{E_{CO}}$ as low as 10 keV have been reported previously, but must be treated with caution as curvature in the spectrum due to the blackbody may have been modelled as Comptonization down-curving. Our observation of down-curving strongly justifies the use of a Comptonizing term in the two-component model; the present work with good fits for progressive covering, and previous work, show that this is extended emission, and therefore there is little doubt that it originates in the ADC. We have found that the cut-off energy is ∼80 keV, implying an average electron temperature $\mathrm{kT_e}$ in the Comptonizing region of ∼ 30 keV. From $\Gamma$, we derive a Comptonisation y-parameter of 1.82, and from the y-parameter $\mathrm{kT_e}$ relation, an optical depth, $\tau$, of 2.8 and hence, an average column density in the ADC of $4.2 \times 10^{24}$ H atom cm$^{-2}$ are found. Similar values were obtained by Sunyaev-Titarchuk modelling.

The spectral fitting results may be used to estimate the sizes of the emission regions as follows. For the blackbody, the unabsorbed flux in the band 0.5–200 keV is $5.5 \times 10^{-11}$ erg cm$^{-2}$ s$^{-1}$, corresponding to a luminosity $\mathrm{L_{bb}} \sim 5 \times 10^{35}$ erg s$^{-1}$, and a blackbody radius $\mathrm{r_{bb}}$ of 0.76 km (defined by $\mathrm{L_{bb}} = 4\pi\,\mathrm{r_{bb}^2}\,\sigma\,\mathrm{T^4}$ where $\sigma$ is Stefan's constant), equivalent to 0.5% of the total surface area of the neutron star. The diameter, $\mathrm{d_{ADC}}$, of the extended emission region, the ADC, can be estimated from the duration $\Delta$t of dip ingress or egress, which was found to be ∼100 s, individual values varying between 90 and 150 s. The radius of the accretion disk will be≳the circularization radius of $1.9 \times 10^{10}$ cm, and the velocity of the absorbing region is given by $2\,\pi\,\mathrm{r_{disk}}/\mathrm{P}$, where $\mathrm{r_{disk}}$ is the disk radius and P the period, and also by $\mathrm{d_{ADC}}/\Delta\mathrm{t}$. From these, an ADC diameter of $4.1 \times 10^9$ cm can be derived. Thus the corona is a region covering the inner 20% of the accretion disk.

The spectral evolution during dipping is well described by the two-component model with the point source blackbody rapidly absorbed, $\mathrm{N_H}$ increasing to $>6.0 \times 10^{24}$ H atom cm$^{-2}$, and the extended Comptonized emission covered progressively by the absorber. This method of fitting is able to explain dipping in the 1–10 keV energy range as being due primarily to

photoelectric absorption, without the need to invoke substantial electron scattering as often proposed in the "absorbed + unabsorbed" approach. With the present approach, the unabsorbed peak is simply the uncovered part of the Comptonized emission as the absorber moves across the source. Above 10 keV the Thomson cross section becomes larger than the photoelectric absorption cross section, and we may expect some reduction in flux due to scattering. Our results indicate that an energy-independent decrease of flux of up to 15% takes place, but this is not a definite detection of electron scattering.

*Acknowledgements.* The BeppoSAX satellite is a joint Italian-Dutch programme. We thank the staff of the BeppoSAX Science Data Center for help with these observations. M. J. Church and M. Bałucińska-Church thank the Astrophysics Division of ESTEC for their hospitality during a recent visit. T. Oosterbroek acknowledges an ESA Fellowship.

## References

Anders E., Grevesse N., 1989, Geochimica et Cosmochimica Acta 53, 197
Barret D., Vedrenne G., 1994, ApJS 92, 505
Barret D., Grindlay J. E., Strickman M. Vedrenne G., 1996, A&AS 120, 269
Boella G., Chiappetti L., Conti G., et al, 1997, A&AS 122, 327
Church M.J., Bałucińska-Church M., 1993, MNRAS 260, 59
Church M.J., Bałucińska-Church M., 1995, A&A 300, 441
Church M.J., Dotani T., Bałucińska-Church M., et al., 1997, ApJ 491, 388
Courvoisier T. J.-L., Parmar A. N., Peacock A., Pakull M., 1986, ApJ 309, 265
Frontera F., Costa E., Dal Fiume D., et al., 1997, A&AS 122, 371
Grindlay J.E., Bailyn C.D., Cohn H., et al., 1988, ApJ 334, L25
Morrison R., McCammon D., 1983, ApJ 270, 119
Parmar A.N., White N.E., Giommi P., Gottwald M., 1986, ApJ 308, 199
Parmar A.N., Martin D.D.E., Bavdaz M., et al., 1997, A&AS 122, 309
Smale A.P., Mason K.O., White N.E. Gottwald M., 1988, MNRAS 232, 647
Smale A.P., Mason K.O., Williams O.R., Watson M.G., 1989, PASJ 41, 607
Smale A.P., Mukai K., Williams O.R., Jones M.H. Corbet R.H.D., 1992, ApJ 400, 330
Walter F.M., Bowyer S., Mason K.O., et al., 1982, ApJ 253, L67
White N.E., Swank J.H., 1982, ApJ 253, L66
White N.E., Parmar A.N., Sztajno M., et al., 1984, ApJ 284, L9